Omniphobic surface modification of electrospun nanofiber membrane *via* vapor deposition for enhanced anti-wetting property in membrane distillation

Xiao-Qiong Wu [a,b,c,d], Xing Wu [c], Ting-Yu Wang [a,b], Lihua Zhao [e], Yen Bach Truong [c], Derrick Ng [c], Yu-Ming Zheng [a,b,d,**], Zongli Xie [c,*]

[a] *CAS Key Laboratory of Urban Pollutant Conversion, Institute of Urban Environment, Chinese Academy of Sciences, 1799 Jimei Road, Xiamen, 361021, China*
[b] *University of Chinese Academy of Sciences, 19A Yuquan Road, Beijing, 100049, China*
[c] *CSIRO Manufacturing, Private Bag 10, Clayton, Victoria, 3168, Australia*
[d] *CAS Center for Excellence in Regional Atmospheric Environment, Institute of Urban Environment, Chinese Academy of Sciences, 1799 Jimei Road, Xiamen, 361021, China*
[e] *Shenzhen Key Laboratory of Environmental Chemistry and Ecological Remediation, College of Chemistry and Environmental Engineering, Shenzhen University, Shenzhen, 518060, China*

A R T I C L E   I N F O

A B S T R A C T

Membrane distillation (MD) is a promising technology for treating saline industrial wastewater, but current hydrophobic MD membranes suffer significant wetting issues due to contaminants commonly present in wastewater. In this study, we report an effective method to fabricate a polyvinylidene fluoride-*co*-hexa-fluoropropylene (PVDF-HFP) electrospun nanofiber membrane with improved anti-wetting property against low-surface-tension substances. Without surface activation, the pristine electrospun nanofiber PVDF-HFP membrane with intrinsic re-entrant structure was directly fluorinated by 1H, 1H, 2H, 2H-perfluorodecyltrichlorosilane (FDTS) employing vapor deposition (VD). The fluorinated membrane exhibited excellent surface omniphobicity with high water and ethanol contact angle of 154.1 ± 0.1° and 122.6 ± 1.7°, respectively. The fluorinated membrane showed highly stable omniphobicity and mechanical properties at harsh conditions such as ultrasonic, boiling water, acid and base treatment. More importantly, the resultant omniphobic membrane exhibited robust wetting resistance to the saline feed containing sodium dodecyl sulfate (SDS, 0.4 mM) in an 8-h dynamic direct contact MD (DCMD) test. This study provides an effective and benign approach to fabricate omniphobic nanofiber membranes which have great potential in treating saline wastewater containing low surface tension substances.

1. Introduction

Membrane distillation (MD) is a hybrid thermal/membrane separation process based on the principle of vapor-liquid equilibrium [1,2]. In a MD process, vapors generated in the hot feed side pass through the hydrophobic membrane pores, then condense into liquids on the cold permeate side. The driven force of the vapor transfer is the trans-membrane vapor pressure gradient triggered by temperature difference. Theoretically, non-volatile solutes can be 100% rejected since the microporous hydrophobic MD membrane only allows volatiles to pass through [3,4]. Moreover, as the vapor pressure is not significantly affected by the salt concentration, MD can desalinate hypersaline water such as reverse osmosis (RO) brine and highly saline industrial wastewater [5–9]. For last decades, MD has been proposed as a promising alternative of other pressure-driven membrane separation processes such as RO for water recovery from highly saline water owing to its unique features of low operating pressure, low sensitivity to feed salinity, 100% theoretical solute rejection and the ability to utilize low-grade thermal energy [1,10].

In a MD system, the hydrophobic microporous membrane plays a

crucial role in vapor transport and preventing direct liquid penetration into the distillate. The most typical MD membranes are made of hydrophobic materials such as polyvinylidene fluoride (PVDF), polypropylene (PP), and polytetrafluoroethylene (PTFE) *via* phase inversion and/or thermal stretching [3,11]. The MD performances of these membranes are acceptable when treating relatively "clean" saline feeds such as seawater and industrial wastewater that contain no low-surface-tension contaminants [12]. However, when used to treat challenging saline industrial wastewater containing low-surface-tension contaminants, these membranes will suffer from wetting issues. For example, surfactants would reduce the surface tension of the feed and/or absorb onto the hydrophobic membranes to render them hydrophilic, and thereby lead to membrane wetting [13]. The consequence of membrane wetting is the direct permeation of feed water into the distillate stream and significantly deteriorate the quality of the distillate [11,14].

In recent years, novel omniphobic membranes have been developed to overcome the wetting issues in MD processes especially induced by low-surface-tension substances [8,15,16]. In 2014, Lin and co-workers first developed the omniphobic membrane for MD applications [8]. In their study, a five-step method was employed to fabricate a glass fiber-based omniphobic membrane. SiO$_2$ nanoparticles (NPs) were first immobilized onto the glass fiber, then surface fluorination and polymer coating were carried out. Compared to the hydrophobic PTFE membrane which was easily wetted at a low sodium dodecyl sulfate (SDS) concentration (0.1 mM), the as-prepared omniphobic membrane showed robust performance in direct contact MD (DCMD) at a high SDS concentration (0.4 mM).

Omniphobic membranes must meet two requirements: re-entrant surface texture and ultralow surface energy. Re-entrant surface textures are geometries that possess overhang structures where the cross-sectional shapes become narrower near the base surface [17]. Re-entrant surface textures can be mushroom, spherical, cylindrical and inverse trapezoidal structures, etc. As shown in Fig. 1A, with re-entrant surface textures, the net traction on the liquid-solid-vapor interface is upward, thus to prevent the intrusion of the liquid into the next level solid surface and support a composite solid-liquid-air interface (i.e. Cassie-Baxter state, Fig. 1B) [18]. In most cases, in order to resist wetting of low-surface-tension liquids, multi-scale re-entrant surface textures were fabricated to maintain a Cassie-Baxter state. Generally, SiO$_2$ NPs [12,13,19], ZnO NPs [20] and Ag NPs [21] were employed to disperse on the surface of porous nanofiber membranes to provide secondary re-entrant surface textures. However, the fabrication process of nanostructure-modified membranes is usually complicated and time-consuming since pre-treatment of substrates is needed to ensure the strong interaction between the nanostructures and substrates. For example, to grow ZnO nanorod arrays on the membrane surface, the PVDF membrane was first dip-coated using zinc acetate ethanol solution and then dried for 20 min. The dried membrane was subsequently immersed into a sodium hydroxide ethanol solution and dried for another 20 min. After rinsed by water and dried at 125 °C, the above-mentioned seed-coating process needed to repeat another 2 times and at least 20 h was needed to form final ZnO nanorod arrays [22].
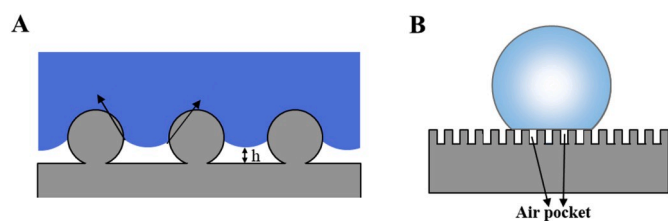
Electrospun nanofibers with a cylindrical shape having intrinsic re-entrant surface textures are ideal to fabricate omniphobic MD membrane. In addition, membranes fabricated by electrospinning usually show interconnected porous network, high porosity, low tortuosity, controllable pore size and suitable membrane thickness which would be beneficial to MD performance [23–28]. Therefore, if we can take advantage of the intrinsic re-entrant structure of electrospun nanofiber membranes without creating additional scale of re-entrant structure, the fabrication of omniphobic electrospun nanofiber membranes will be much more convenient and economic.

On the other hand, to attain ultralow surface energy, fluorinated components such as fluoropolymer, fluorosilane, fluorothiol, fluoroplasma and fluorosurfactant were often used. This is because fluorine is highly electronegative and has low polarizability, which leads to weak cohesive and adhesive force, making it a good choice for creating materials with low surface energy [17]. The most commonly used fluorination strategy is using fluorosilane by dip-coating [18]. Nevertheless, the dip-coating is not an ideal technique for large-scale membrane fabrication because the utilization rate of the coating materials is relatively low and it usually needs multiple coating cycles to graft fluorine-containing substances onto the membrane surface, which is laborious [13,20,29]. Another fluorination method is vapor deposition (VD) which is more convenient and can form a thinner fluorinated layer compared to the dip-coating method. However, for both fluorination methods, surface activation processes (e.g., via alkali treatment, UV or plasma) before fluorosilane deposition are inevitable to generate –OH to form covalent bonds between the fluorisilane and the substrate [17]. To date, few studies have considered to skip the surface activation process by taking advantage of the physical affinity between the long fluoroalkyl chains in fluorosilane and the fluorine-containing substrates [30,31]. All in all, the fabrication processes of omniphobic membranes by multiple steps of nanostructure modification, surface activation and fluorination reported in previous studies were usually time-consuming and complicated [8,15,16,20,32]. Thus, simpler method for fabricating omniphobic membranes is required.

Herein, we report an facile and effective method to fabricate omniphobic polyvinylidene fluoride-co-hexafluoropropylene (PVDF-HFP) nanofiber membrane with robust anti-wetting property. In our strategy, the nanofiber membrane with intrinsic re-entrant structure was first fabricated by electrospinning. Subsequently, without surface activation, facile and convenient VD of 1H, 1H, 2H, 2H-perfluorodecyltrichlorosilane (FDTS) on physical basis instead of chemical bonding was applied to lower the surface energy of the membrane. The fluorination process was optimized including fluorination time, fluorination temperature and FDTS amount. The morphology, characteristics and wetting property of the fluorinated PVDF-HFP membrane were investigated and compared with the initial PVDF-HFP membrane to evaluate the effectiveness of this VD fluorination method. In addition, the stability of the omniphobicity was also investigated by challenging the fluorinated membrane in critical conditions. Moreover, direct contact MD (DCMD) experiments were carried out by using 3.5 wt% NaCl solution containing 0.4 mM SDS as feed to investigate the feasibility of the fluorinated membrane to desalinating low surface tension saline wastewater.

2. Experimental

2.1. Materials

Polyvinylidene fluoride-*co*-hexafluoropropylene (PVDF-HFP; Mw = 400,000 g mol^{-1}) was purchased from Sigma-Aldrich, St Louis, USA. SDS (90%) was bought from MERCK, Germany. N, N-dimethylformamide (DMF) of HPLC grade was commercially available from VWR International, Pty Ltd., Australia. Ethanol and sodium chloride (NaCl) of analytical grade were purchased from EMSURE®, Germany. Acetone, isopropanol (IPA) and n-decane (CH$_3$(CH$_2$)$_8$CH$_3$) were brought from EMD Millipore Corporation, USA. 1H, 1H, 2H, 2H-

Fig. 1. Schematic illustrating the composite liquid-solid-vapor interface on re-entrant structure (using cylindrical fibers as example) (A) and liquid droplet on rough surface in a Cassie-Baxter wetting state (B).

perfluorodecyltrichlorosilane ($CF_3(CF_2)_7CH_2CH_2SiCl_3$, FDTS) was obtained from Gelest, INC, USA. All chemicals were used as-received without further purification.

2.2. Membrane fabrication and surface modification

2.2.1. Electrospinning

As shown in Fig. 2, the omniphobic nanofiber membranes were firstly fabricated by electrospinning and then fluorinated through a VD process. To prepare PVDF-HFP dope solution, 15 wt% of PVDF-HFP tablets was dissolved in a DMF/acetone mixture with a weight ratio of 4:1 under continuous stirring at room temperature for 24 h. 0.025 wt% of LiCl was added to the solution to improve the spinnability of PVDF-HFP solution.

Prior to electrospinning, the dope solution was firstly degassed for 2 h before being transferred to a 12-mL syringe (TERUMO Philippines corporation, Taipei) with a 23G needle (TERUMO Philippines corporation, Taipei). The feeding rate of the solution was controlled at 1 mL h^{-1} by a syringe pump (Braintree Scientific, Inc., US). The voltage and distance between the needle tip and the grounded rotating drum wrapped with an aluminum foil were set as 17.5 ± 0.5 kV and 15 cm, respectively. The membrane thickness was controlled by electrospinning time. The humidity and temperature in the electrospinning chamber were 40–50% and 21–22 °C, respectively. The details of the electrospinning set-up were described in a previous study [33]. Prior to fluorination, the pristine PVDF-HFP membrane was placed in a vacuum oven at 60 °C overnight for removing the residual solvent.

2.2.2. Surface modification by fluorination

A membrane with a size of 150×110 mm was placed on a sample holder in a desiccator. Then, the uncovered desiccator was put in a glovebox by purging with N_2 for about 1 h. 50–400 μL of FDTS was added into a PTFE container under the membrane, then the desiccator was sealed by lid using vacuum grease in the glovebox under N_2 atmosphere. The desiccator was then taken out from the glovebox and placed in a vacuum oven for 5–40 h with the vacuum degree of 20 kPa at the temperature of 50–120 °C. The fluorinated membranes from the PVDF-HFP membrane were labeled as the PVDF-HFP-F membrane as shown in Fig. 2.

2.3. Membrane characterization

The top surface and cross-sectional morphology and elemental mappings of the membranes were investigated using a scanning electron microscopy (SEM, Merlin Zeiss Gemini 2) associated with an energy dispersive X-ray spectra (EDS) system. The samples were sputtered by Iridium for 50 s before SEM observation.

Surface chemical compositions and functional groups of the membranes before and after fluorination were analyzed by an attenuated total reflection Fourier transform infrared (ATR-FTIR) spectrometer (Thermo Scientific NICOLET 6700) in the wavelength range of 4000-650 cm^{-1}. The chemical compositions and valence states of the constituent elements were determined by an X-ray photoelectron spectrometer (XPS; AXIS SUPRA, KARTOS/SHIMADZU, Japan) with a 150 W monochromatic Al Kα source. The binding energy of carbon 1s electron (284.8 eV), corresponding to graphitic carbon was used to calibrate the scan spectra. The surface topography and roughness of the membranes was evaluated using a Dimension 3100 atomic force microscopy (AFM, Bruker icon, USA) with a scanning area of 3 μm × 3 μm. An arithmetic average roughness (Ra) was calculated over the scanning area.

The membrane thickness was determined from the cross-sectional SEM image of the membrane. The pore size distributions of the membranes were determined by a Porometer 3G instrument. Before testing, the sample was first wetted by Porofil (a low-surface-tension wetting liquid, 16 mN m^{-1}). Subsequently, N_2 gas was applied to test the wet and dry curves which can deduce pore size and pore size distribution. The porosity of the membranes which was defined as the pore volume of the membrane divided by the total volume of the membrane was tested by the gravimetric method and calculated by the following equation:

$$\tau = \frac{(m_{wet} - m_{dry})/\rho_{IPA}}{(m_{wet} - m_{dry})/\rho_{IPA} + m_{dry}/\rho_{mat}} \tag{1}$$

where m_{wet} and m_{dry} are the mass of wet and dry membrane, respectively. ρ_{IPA} is the density of isopropanol (0.786 g cm^{-3}) and ρ_{mat} is the density of the material ($\sim$1.77 g cm^{-3}).

In order to investigate the wettability of the membranes, the contact angles of DI water, 3.5% NaCl solution containing 0.4 mM SDS, n-decane and ethanol were measured by a contact angle instrument (KSV tensiometer contact angle instrument) using the sessile drop method. Digital images of the droplets were recorded using a camera and the values of the contact angle were analyzed by the curve fitting method. The average value of the contact angle was determined by the values of at least 3 different positions for each membrane. The liquid entry pressure (LEP) measurement was conducted with a cylindrical pressure dead-end filtration cell with an effective surface area of 10.2 cm^2 connected to a pressurized air bottle via a pressure regulator and a gauge. A dry PVDF-HFP or PVDF-HFP-F membrane was fixed at the bottom of the filtration cell followed by pressurizing 100 mL deionized (DI) water with air as feed. The pressure started from 20 kPa and gradually increased by 10 kPa every 2 min. LEP was determined as the pressure at which the first droplet of water appeared at the permeate side of the pressure filtration cell. LEP can be calculated by the following equation:

$$LEP = -\frac{4B\gamma_l cos\theta}{d_{max}} \tag{2}$$

where B is a geometric pore coefficient, θ is the contact angle, γ_l is the surface tension of the tested liquid (N m^{-1}), and d_{max} is the maximum pore size of the membrane (m).

2.4. Omniphobicity stability tests

The stability of the PVDF-HFP-F membrane's omniphobicity was tested under the harsh conditions including ultrasonic bath treatment for 60 min (the ultrasonic frequency and power was 40 kHz and 100 W respectively and the membrane was kept immersing in water during the
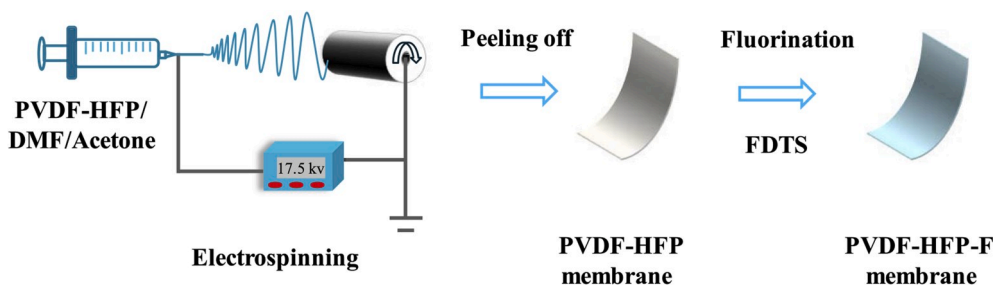

Fig. 2. Schematic of the fabrication process of the fluorinated PVDF-HFP membrane.

treatment), boiling water treatment (DI water, 100 °C) for 60 min, HCl solution (1 M) and NaOH solution (0.5 M) treatment at room temperature for 60 min, respectively. After the treatment, water contact angle (WCA) and ethanol contact angle (ECA) of the membranes were measured.

The surface energies of PVDF-HFP and PVDF-HFP-F electrospun nanofiber membranes were estimated by the Owens−Wendt method using the experimentally determined intrinsic contact angles of water (θ_{Water} with $\gamma_{Water} = 72.8$ mN m^{-1}) and methylene iodide (θ_{MI} with $\gamma_{MI} = 50.8$ mN m^{-1}) [15,34,35]. In Owens-Wendt method, the surface energy (γ_s) is resolved into two components, i.e., dispersion (γ_s^d) and hydrogen bonding-dipole (γ_s^h) ($\gamma_s = \gamma_s^d + \gamma_s^h$), and the γ_s^d and γ_s^h can be calculated by the following equations:

$$(1 + cos\theta_{Water})\gamma_{Water} = 2\sqrt{\gamma_s^d}\sqrt{\gamma_{Water}^d} + 2\sqrt{\gamma_s^h}\sqrt{\gamma_{Water}^h} \tag{3}$$

$$\left((1 + cos\theta_{MI})\gamma_{MI} = 2\sqrt{\gamma_s^d}\sqrt{\gamma_{MI}^d} + 2\sqrt{\gamma_s^h}\sqrt{\gamma_{MI}^h}\right. \tag{4}$$

where θ_{Water} and θ_{MI} are the contact angles of DI water and methylene iodide on the membranes, respectively. γ_{Water} (72.8 mN m^{-1}) and γ_{MI} (50.8 mN m^{-1}) are the surface tensions of DI water and methylene iodide, respectively. γ_{Water}^d (21.8 mN m^{-1}) and γ_{Water}^h (51.0 mN m^{-1}) represent the dispersion and hydrogen bonding-dipole of DI water, respectively, while γ_{MI}^d (49.5 mN m^{-1}) and γ_{MI}^h (1.3 mN m^{-1}) represent the dispersion and hydrogen bonding-dipole of methylene iodide, respectively.

The solid-liquid contact area fractions (f_s) on the PVDF-HFP and PVDF-HFP-F electrospun nanofiber membranes were evaluated by the following equation [36]:

$$f_s = \frac{R \times (2\pi - 2\theta)}{2R + 2D} \times 100\% \tag{5}$$

where R (nm) is the mean radius of the nanofibers; θ (°) is the contact angle of the employed liquid on the nanofiber membrane; 2D (nm) is the distance between the two nanofibers, which is the mean pore size of the nanofiber membrane in the present study.

2.5. Performance tests in DCMD

MD performance of the nanofiber membranes was tested by using a cross-flow DCMD system as shown in Fig. 3. The membrane was sealed between two identical acrylic plates with a size of 150 × 110 mm (L × W) with rubber gasket on them (size: 150 × 110 -115 × 65 mm; thickness: 1.5 mm). The effective area for MD was about 75 cm^2. 2 L of 3.5 wt % NaCl solution containing 0.4 mM SDS was used as the feed solution which was concentrated continuously until the end of the experiment. 1 L of DI water placed on an electronic balance was used as starting permeate solution. A peristaltic pump was applied to maintain the circulation flow rate of the feed and the permeate solution at 350 mL min^{-1} (the equivalent linear flow velocity of 0.06 m s^{-1}). The temperature at

the feed side was controlled at 60 ± 2 °C by using a water bath while the temperature at the permeate side was kept at 10 ± 2 °C by using a chiller. The temperatures at the inlet and outlet of both feed and permeate sides were monitored by four thermocouples. The weight changes in permeate side were recorded by an electronic balance (AND, GF-6000) connected to a computer. The conductivity of the permeate was recorded on line by a conductivity meter (HANNA, HI 98192) to monitor the quality change of the permeate. The water flux (J) for the DCMD test was calculated by the following equation:

$$J = \frac{\Delta m}{S \cdot \Delta t} \tag{6}$$

where Δm (kg) is the weight gain of the permeate during the testing time Δt (h), while S (m^2) is the effective area of the membrane.
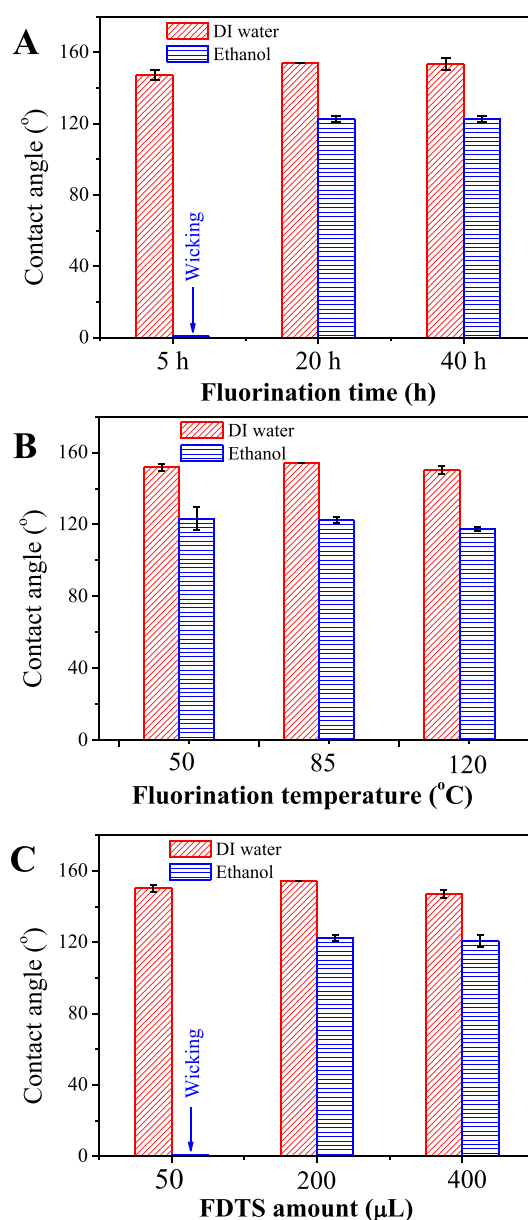

Fig. 4. The effects of fluorination time (A), fluorination temperature (B) and FDTS amount (C) on water contact angles and ethanol contact angles of the PVDF-HFP-F membrane.
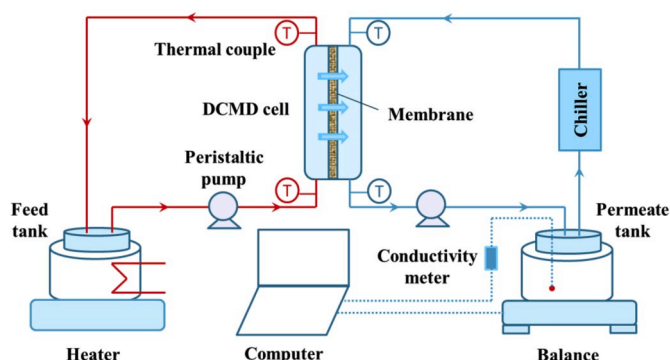

Fig. 3. Schematic of the DCMD set-up.

3. Results and discussion

3.1. Effect of fluorination conditions

To understand the VD fluorination process, the effects of fluorination time (5–40 h), fluorination temperature (50–120 °C) and FDTS amount (50–400 μL) on omniphobicity of the PVDF-HFP-F membrane were investigated. As shown in Fig. 4A, fluorination time could significantly influence the omniphobicity. With short modification time of 5 h, the obtained PVDF-HFP-F membrane could be wicked by ethanol instantly even it possessed high WCA, indicating 5 h is not enough for the complete evaporation of the liquid FDTS. When the modification time increased to 20 h, the corresponding PVDF-HFP-F membrane could successfully obtain omniphobicity as it can resist wetting by both water and ethanol. Further prolonging the fluorination time did not change WCA and ethanol contact angle (ECA) much, which indicated that the VD process might be already completed for 20 h. Fig. 4B shows the effect of fluorination temperature on omniphobicity of the PVDF-HFP-F membrane, which revealed that the influence of the temperature on the omniphobicity of membranes was not significant since FDTS can evaporate at an relatively low temperature of 50 °C. However, the obtained omniphobicity of the membrane at 50 °C was less stable than that of at higher temperatures. The effect of FDTS amount was critical as shown in Fig. 4C. When FDTS was not enough to fully cover the surface (50 μL), the obtained PVDF-HFP-F membrane could not resist to ethanol. After increasing the FDTS amount to 200 μL, the omniphobicity was successfully obtained. This might be attributed to the completely enwrapped of PVDF-HFP nanofibers by FDTS, thus to change the surface energy of the membrane surface. The WCA and ethanol contact angle kept almost unchanged by further increasing the FDTS to 400 μL, suggesting that thicker FDTS layer on nanofiber did not have additional effect on the membrane omniphobicity. Based on the above results, in order to obtain stable and satisfied omnipobicity, the fluorination time, temperature and FDTS amount were set as 20 h, 85 °C and 200 μL, respectively.

3.2. Wetting resistance of the PVDF-HFP-F membrane

The anti-wetting ability of the PVDF-HFP membrane before and after fluorination were compared by measuring the contact angle of four kinds of liquids with different surface tensions (Fig. 5). The four liquids are DI water, 3.5 wt% NaCl solution containing 0.4 mM SDS, n-decane and ethanol with surface tensions of 72.8, <31, 23.8 and 22.1 mN m^{-1}, respectively [37,38]. Owing to the hydrophobic nature of PVDF-HFP and the porous and intrinsic re-entrant structure, the initial PVDF-HFP membrane exhibited a high static WCA of 144.9 ± 0.3°. However, when 3.5 wt% NaCl solution containing 0.4 mM SDS (<31 mN m^{-1}) was
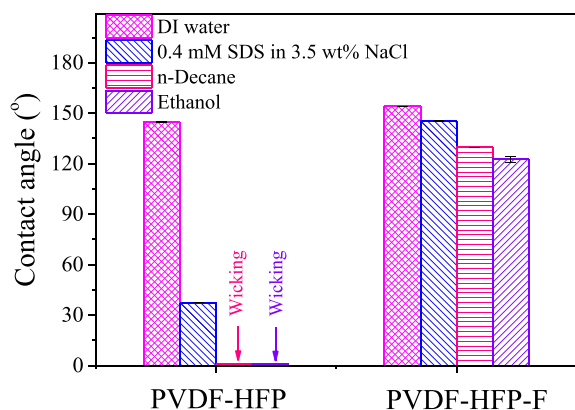
Table 1
The contact angles and surface energies of the PVDF-HFP and PVDF-HFP-F membranes.

Sample	Contact angle (°)		Surface energy (mN m^{-1})		
	Deionized water	Methylene iodide	γ_{sv}^d	γ_{sv}^p	γ_{sv}
PVDF-HFP	144.9 ± 0.3	136.4 ± 1.9	0.895	0.095	0.990
PVDF-HFP-F	154.1 ± 0.1	146.0 ± 1.3	0.357	0.015	0.372

used, the contact angle was only 37.4 ± 0.1°. Even worse, the PVDF-HFP membrane was instantly wicked by low-surface-tension liquids, i.e. n-decane and ethanol though PVDF-HFP membrane possesses intrinsic re-entrant structures, which indicated that the surface energy of PVDF-HFP was not low enough to resist low-surface-tension solvent.
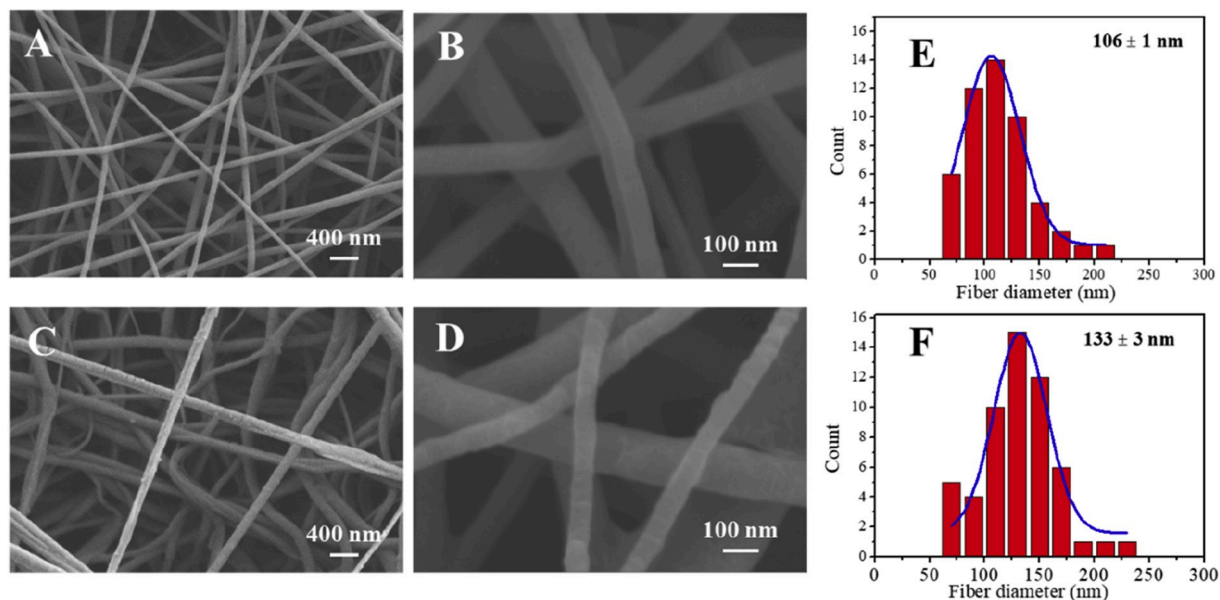
After fluorination, the PVDF-HFP-F membrane exhibited superhydrophobicity with a WCA of 154.1 ± 0.1°. In addition, the PVDF-HFP-F membrane can resist wetting to 3.5 wt% NaCl solution containing 0.4 mM SDS, n-decane and ethanol with contact angles of 145.4 ± 0.2°, 129.7 ± 0.1° and 122.6 ± 1.7°, respectively, which may result from the successful deposition of FDTS with low surface energy (Table 1). In order to better demonstrate the superhydrophobicity and omniphobicity, the contact angles of DI water and ethanol droplets on PVDF-HFP-F membrane with increasing time were shown in Fig. S1. It can be seen that WCAs remain almost the same as the initial value after 5 min and ECAs slightly decrease after 2 min mainly due to the rapid evaporation of ethanol (See inset in Fig. S1B). The above results indicated that the simple VD of FDTS on nanofiber membrane surface could be an effective strategy to fabricate omniphobic membrane by combination of the intrinsic re-entrant surface texture of the nanofiber membrane and the low surface energy originating from surface fluorination.

3.3. Membrane morphology

Fig. 6A illustrates the morphological characteristic of the pristine electrospun PVDF-HFP nanofiber membrane, which is composed of long, continuous, cylindrical and randomly distributed nanofibers. The nanofibers were beadless and relatively uniform with an average diameter of 106 ± 1 nm (Fig. 6E). Comparing the PVDF-HFP-F membrane with the PVDF-HFP membrane, the interconnected nanofibrous network structure of the membrane was hardly changed after fluorination (Fig. 6C). As illustrated in Fig. 6B and 6D, after fluorination, the surface feature of nanofibers in the PVDF-HPF-F membrane were affected and the nanofibers became rougher, which caused the increase of Ra value in the PVFD-HFP-F membrane (Fig. S2). In addition, compared to the PVDF-HFP membrane, the average nanofiber diameter of PVDF-HFP-F membrane increased to 133 ± 3 nm (Fig. 6F). The increase in the mean nanofiber diameter might be attributed to combined effects of thermal expansion of the nanofibers caused by heating [31] and the successful deposition of FDTS on PVDF-HFP nanofiber surface. To further verify the successful coating of FDTS, element mappings of PVDF-HFP and PVDF-HFP-F membrane was obtained by SEM-EDS. As shown in Fig. S3 form the Map Sum Spectrum, the ratios of F, O and Si increased after VD fluorination process, which was resulted from the successful surface deposition of FDTS. However, the uniformity of the FDTS coating cannot be clearly evaluated by the EDS detection because the pristine PVDF-HFP also contains F and the noises of Si and O was relatively strong due to their low contents.

3.4. Structural properties of membranes

The change in structural properties of the PVDF-HFP membrane before and after fluorination were investigated from the aspects of thickness, porosity, mean pore size and LEP. As can be seen from the cross-sectional images in Fig. 7, the membrane thickness increased from 85 to 112 μm after fluorination. The increase of thickness may result from the increased fiber diameters caused by thermal expansion and the

Fig. 5. Contact angles of DI water, 0.4 mM SDS in 3.5 wt% NaCl, n-decane and ethanol on PVDF-HFP and PVDF-HFP-F membranes.

Fig. 6. SEM images of the top surface of PVDF-HFP (A and B), PVDF-HFP-F (C and D) membranes and the corresponding fiber diameter distributions of PVDF-HFP (E), PVDF-HFP-F (F) membranes.
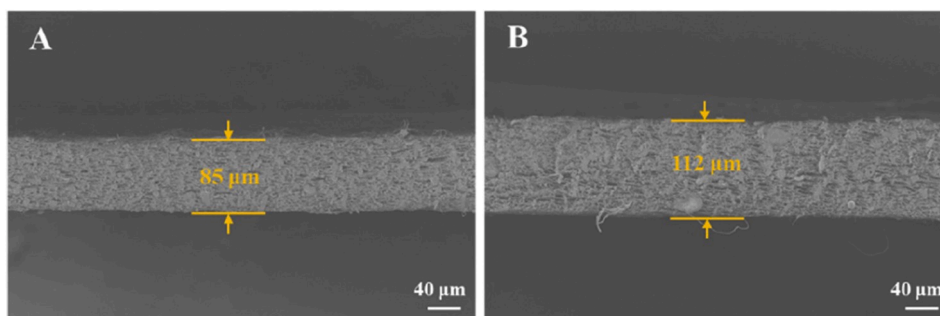
Fig. 7. The cross-sectional SEM images of PVDF-HFP (A), PVDF-HFP-F (B) membrane, and their corresponding thickness.
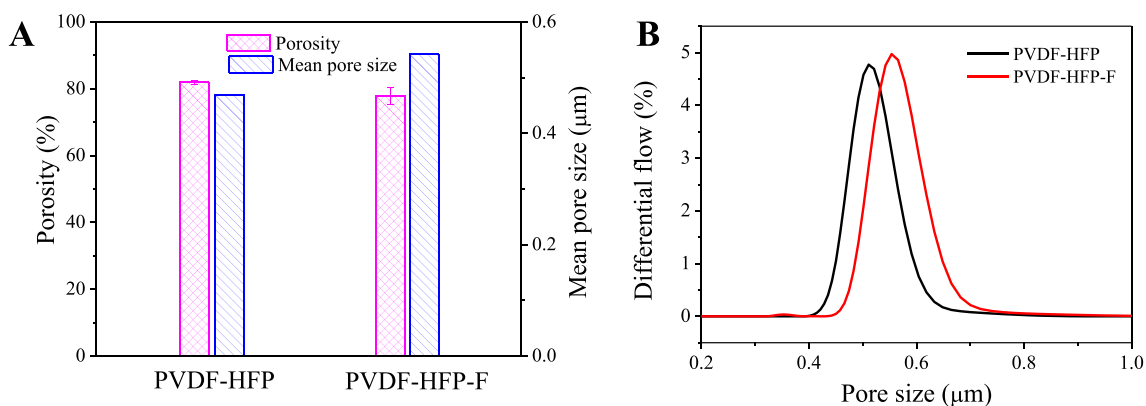
Fig. 8. Porosity and mean pore size (A) and pore size distribution (B) of PVDF-HFP and PVDF-HFP-F membranes.

successful deposition of FDTS on the nanofiber surface.

Fig. 8A shows the porosity of the membranes before and after fluorination. Benefiting from the interconnected porous structure, both the PVDF-HFP and PVDF-HFP-F membrane exhibited a relatively high porosity above 78%. Compared with the PVDF-HFP membrane, the porosity of the PVDF-HFP-F membrane decreased insignificantly. This result suggests that VD fluorination process is better than the liquid immersion method because the latter method was reported to decrease the membrane porosity to some extent [30,39].

As shown in Fig. 8A and Table 2, the mean pore size of the PVDF-HFP-F membrane was 0.55 μm, which was larger than that of PVDF-HFP membrane (0.47 μm). The larger mean pore size of PVDF-HFP-F membrane may result from the increase of the fiber diameter caused by fluorination since pore size of an electrospun nanofiber membrane is increased linearly with the fiber diameter [40]. Specifically, the mean pore size was 4.0–4.5 times the mean fiber diameter (Table 2), which

Table 2
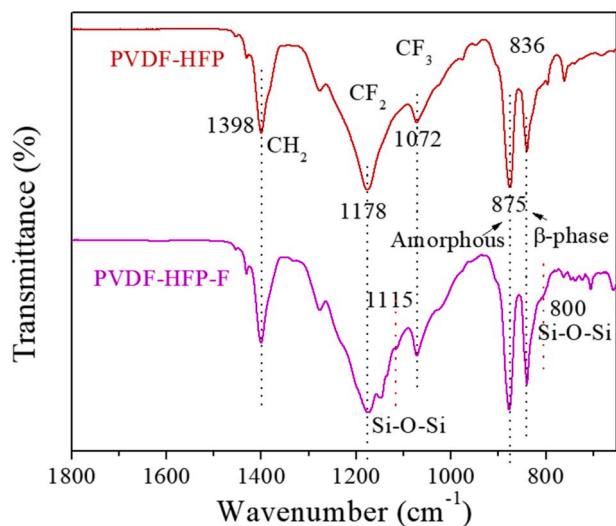Pore sizes, mean fiber dimeters and their corresponding relationships of the fabricated membranes.

Membrane	Min[a], µm	Mean[b], µm	Max[c], µm	MFD[d], nm	Mean/MFD
PVDF-HFP	0.41	0.47	0.65	106 ± 1	4.42
PVDF-HFP-F	0.39	0.55	0.78	133 ± 3	4.08

[a] Minimum pore size.
[b] Mean pore size.
[c] Maximum pore size.
[d] Mean fiber diameter.

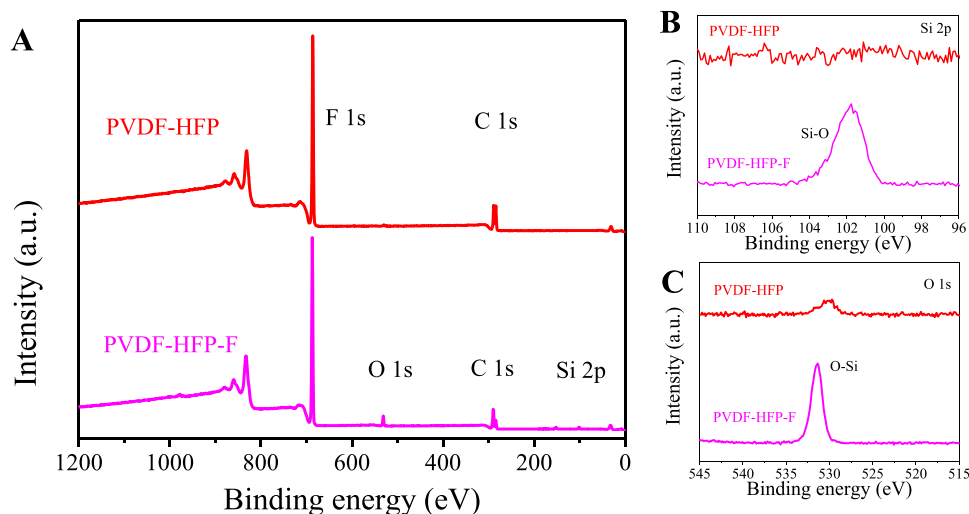**Fig. 9.** ATR FTIR spectra of PVDF-HFP and PVDF-HFP-F membranes.

was consistent with that of the cellulose nanofiber membrane [40]. Besides, it could be seen from Fig. 8B that the pore size distributionof PVDF-HFP-F membrane shifted to right compared to that of PVDF-HFP membrane, which might be beneficial to maintain the DCMD performance of PVDF-HFP-F membrane. Moreover, the LEP of the PVDF-HPF membrane increased from 1.65 to 2.25 bar after fluorination, which mainly resulted from the increase of contact angles of the PVDF-HFP membrane according to the equation (2).

3.5. Physical and chemical properties of the membrane surface

The surface compositions and functional groups of the membranes were investigated by ATR-FTIR spectroscopy. As shown in Fig. 9, several characteristic peaks assigned to PVDF-HFP were identified from the spectra of the PVDF-HFP membrane. Peaks at 1398, 1178 and 1072 cm^{-1} were attributed to the wagging of CH_2, antisymmetric stretching of CF_2 and out-of-plane deformation of CF_3, respectively. The strong peaks located at 875 and 836 cm^{-1} were assigned to amorphous and β-phase of the PVDF-HFP, respectively [16]. Except for these characteristic peaks for PVDF-HFP, there are two new peaks emerging on the curves of the PVDF-HFP-F membrane. The new peaks at 1115 and 800 cm^{-1} was originating from Si–O–Si stretching vibration [30], which suggests that FDTS hydrolyzed and polycondensated on the surface of nanofiber generating polysiloxane networks.

The surface chemical compositions of the PVDF-HFP and PVDF-HFP-F membranes were also analyzed by XPS. The survey spectra in Fig. 10A revealed that fluorine (685.8 eV for F 1s) and carbon (286.8 eV for C 1s) elements existed in both membranes while silica (101.8 eV for Si 2p) and oxygen (531.5 eV for O 1s) elements existed only in PVDF-HFP-F membrane, which can be further verified by the Si 2p and O 1s spectra (Fig. 10B and C). The strong Si-O and O-Si peaks in PVDF-HFP-F membrane again confirmed the hydrolysis and polycondesation of FDTS and the formation of polysiloxane networks on the nanofiber surface.

The resultant structures and properties of the as-prepared omni-phobic membrane were associated with the FDTS depositing mechanism on the nanofiber surface (Fig. 11). During the process of VD fluorination, since there is no –OH on PVDF-HFP nanofiber surface, the FDTS vapor molecule with a long fluoroalkyl chain which has low polarity tend to physically adsorb on the hydrophobic PVDF-HFP nanofiber surface, exposing the highly moisture-sensitive trichlorosilane head outside [41]. The active trichlorosilane heads exposing outwards easily hydrolyze by using trace moisture in the desiccator. Then, the intermolecular polycondensation could take place among the hydrolyzed FDTS molecules to form polysiloxane networks with the long fluoroalkyl chain exposing to the surface to gain the lowest system energy [42]. Moreover, the water molecular produced by polycondensation can induce the hydrolysis of other FDTS molecule thus to facilitate the deposition process throughout the PVDF-HFP nanofiber membrane [30]. As a consequence, the successful deposition of FDTS on PVDF-HFP nanofiber surface, together with the intrinsic re-entrant texture of PVDF-HFP nanofiber result in omniphobicity.

Fig. 10. Surface XPS survey scans (A), Si 2p XPS spectra (B) and O1s XPS spectra of PVDF-HFP and PVDF-HFP-F membranes.
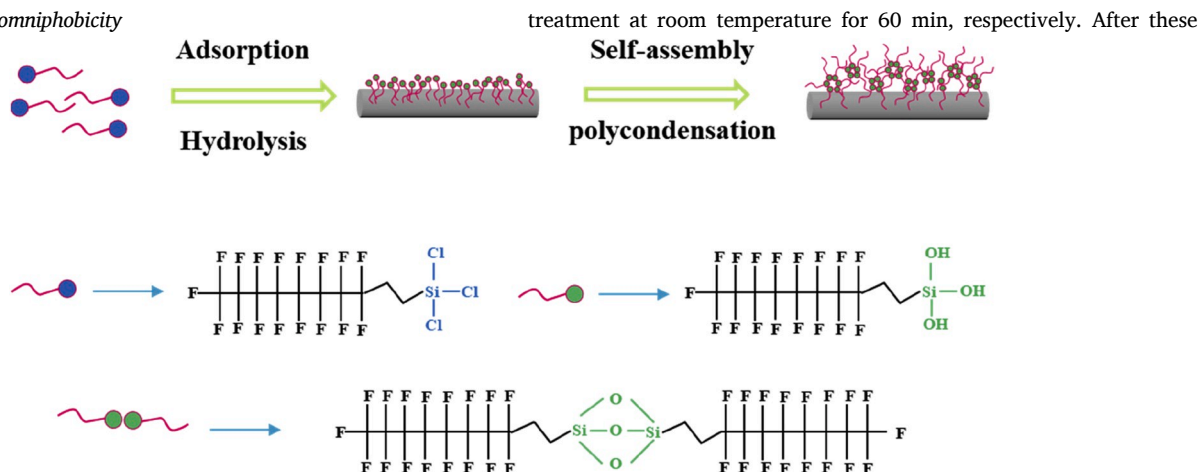
3.6. Stability of the omniphobicity

treatment at room temperature for 60 min, respectively. After these

Fig. 11. Schematic illustration of possible interaction mechanism between FDTS and PVDF-HFP nanofibers by the VD fluorination process.
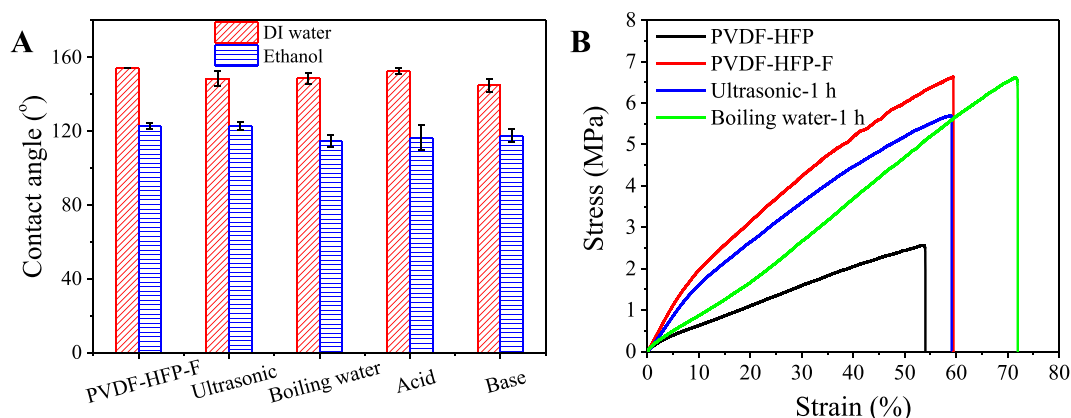

Fig. 12. (A) WCAs and ECAs of the PVDF-HFP-F membrane before and after treated by ultrasonic, boiling water, 1 M HCl and 0.5 M NaOH for 60 min, respectively. (B) The mechanical properties of PVDF-HPF membrane, PVDF-HFP-F membrane and the PVDF-HFP-F membranes by 1-h ultrasonic treatment and 1-h boiling water treatment.
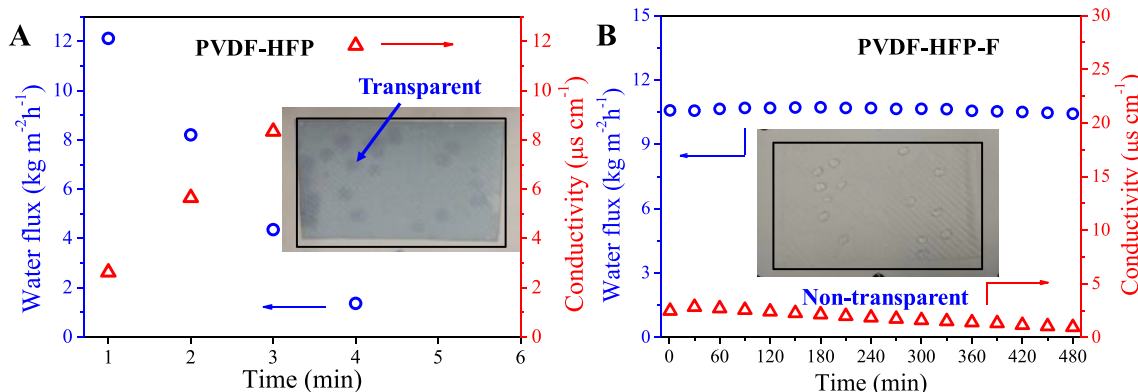

Fig. 13. (A) Conductivity and water flux verses time of the PVDF-HFP membrane (A) and PVDF-HFP-F membrane (B) in DCMD processes using 3.5 wt% NaCl solution containing 0.4 mM SDS as feed solution. Temperature difference was 50 °C and the flow rate was 350 mL min⁻¹ for both feed and permeate side. The pictures inserted in A and B are the PVDF-HFP and PVDF-HFP-F membrane after tests.

As there is no chemical bond between FDTS and PVDF-HFP nanofibers, doubt will be arisen whether the physical interaction is stable enough for practical application. In order to investigate the stability of the omniphobicity of the PVDF-HFP-F membrane, harsh conditions were employed to challenge the PVDF-HFP-F membrane which included ultrasonic bath treatment for 60 min, boiling water treatment (DI water, 100 °C) for 60 min, HCl solution (1 M) and NaOH solution (0.5 M)

treatments, WCAs and ECAs of those treated membranes were determined and compared with untreated PVDF-HFP-F membrane. The results shown in Fig. 12A reveal that the WCAs and ECAs hardly changed and kept at about 145° and 115°, respectively, which indicated that the PVDF-HFP-F membrane fluorinated by the simple VD method on the physical basis is stable and has great potential to be applied in harsh conditions. To further investigating the stability of the PVDF-HFP-F

Table 3

The comparison of the modification method and performance in DCMD of PVDF-HFP-F membrane with those of other omniphobic membranes reported in previous studies.

Membrane	Modification method	Effective area (cm^2)	Saline feed NaCl	T (°C)	SDS concentration-Testing time	Flux (L m^{-2}h^{-1})	Reference
Glass fiber	APTES treatment + SiNPs coating + SiCl$_4$ treatment + dip-coating FAS/hexane + PVDF-HFP/FAS coating + heat treatment	12	1 M	60/20	0.1 mM-2 h 0.2 mM-2 h 0.3 mM-2 h 0.4 mM-1 h	15.8 ± 2.7	[8]
PVDF nanofiber	THF-PDMS-PVDF Electrospraying	9.8	3.5 wt%	60/20	1.1 mM-4 h 1.2 mM-wetting	NA	[10]
PVDF-HFP nanofiber	Dip-coating with SiNPs + FDTS silanization + thermal annealing	20	1 M%	60/20	0.1 mM-2 h 0.2 mM-2 h 0.3 mM-2 h	~10	[16]
PVDF flat sheet	Alkaline treatment + APTES grafting + SiNPs coating + FDTS coating	20	1 M	60/20	0.05 mM-2 h 0.1 mM-2 h 0.2 mM-2 h	~10–11^c	[32]
Glass fiber	Surface activation + ZnO NPs deposition + dip-coating in FAS17/n-hexane + PVDF-HFP/FAS17 coating	10.74	1 M	60/20	0.3 mM-8 h	~11–12^c	[20]
PVDF nanofiber	FTCS/n-hexane solution immersion + heat treatment	30	3.5 wt%	60/20	0.05 mM-2 h 0.1 mM-2h	NA	[30]
PVDF-HFP nanofiber	Heat press + dip-coating in FAS/hexane + heat treatment	27.39	3.5 wt%	65/25	0.1 mM-1 h	~15^c	[31]
PVDF-HFP nanofiber	One-step vapor deposition of FDTS	75	3.5 wt%	60/10	0.4 mM-8 h	10.5	This work

NA presents not available; C represents calculation from the figure.

membrane, the mechanical strength of PVDF-HFP-F membranes after ultrasonic treatment and hot water treatment were tested (Fig. 12B and Fig. S4). The result indicates that the mechanical stability of the PVDF-HFP-F membrane can be maintained after harsh ultrasonic bath and boiling water treatments for 1 h. As shown, both the strain and tensile stress of the PVDF-HFP membrane were significantly enhanced by the VD fluorination process. The tensile stress of PVDF-HFP-F was about 6.6 MPa and the corresponding strain was about 59% while the tensile stress of PVDF-HFP was about 2.6 MPa and the corresponding strain was about 54%. After ultrasonic treatment for 1 h, the tensile stress just slightly decreased (5.7 MPa) and the strain was unchanged. After boiling water treatment for 1 h, the tensile stress kept the same with PVDF-HFP-F while the strain increased from 59% to 72% which may be caused by the slight shrinking of the membrane in the high temperature.

3.7. Anti-wetting performance in DCMD

To investigate the anti-wetting performance of the omniphobic membrane in DCMD, 0.4 mM SDS was introduced to 3.5 wt% NaCl solution to lower the surface tension of the feed solution (<31 mN m^{-1}). When testing the performance of the PVDF-HFP membrane, it was found that PVDF-HFP membrane was wetted very quickly before reaching a steady-state and the conductivity of the permeate solution began to increase at the beginning of the test (Fig. 13A). Besides, the membrane became transparent after the test (Inserted picture of Fig. 13A), which again confirmed the wetting of the membrane. This result suggested that the hydrophobic PVDF-HFP membrane cannot resist wetting by low surface tension feed in DCMD.

Be different form the PVDF-HFP membrane, the omniphobic PVDF-HFP-F membrane exhibited excellent wetting resistance to this low surface tension feed in the same DCMD process. As can be seen in Fig. 13B, during an 8-h test, the water flux of the PVDF-HFP-F membrane was maintained at around 10.5 kg m^{-2} h^{-1}, and the conductivity kept lower than 3 μs cm^{-1}. After the test, the PVDF-HFP-F membrane was still non-transparent and hydrophobic, as shown in the inset photograph in Fig. 13B. It should be noted that the average DI water flux decreased marginally from 14.4 kg m^{-2}h^{-1} of the PVDF-HFP membrane to 12.1 kg m^{-2}h^{-1} of the PVDF-HFP-F membrane (Fig. S5), showing that this VD fluorination could well maintain the water flux while improving the wetting resistance property. The results suggested that the omniphobic

PVDF-HFP-F membrane had potential application in treating saline wastewater containing low-surface-tension substances. Table 3 lists the comparison of the modification method and performance in DCMD of PVDF-HFP-F with those of other omniphobic membranes reported in previous studies. As can be seen from Table 3, the performance in DCMD of desalinating saline water containing low-surface-tension substances of the omniphobic PVDF-HFP-F membrane was comparable with other omniphobic membranes developed in previous studies, especially in light of the facile and effective modification method.

The anti-wetting properties of the PVDF-HFP-F membrane was mainly attributed to the cooperation of the intrinsic re-entrant structures of electrospun nanofiber membrane and the low surface energy resultedfrom the successful deposition of FDTS on the nanofiber surface. In principle, the feed solution containing surfactants could readily intrude into pores of the PVDF-HFP membrane since the existence of surfactants resulted in a low surface tension of the feed solution. The contact area of feed solution and membrane was relatively large as a result of the low surface tension of the feed solution and the high surface energy of the PVDF-HFP membrane, which facilitated the transportation of feed solution into the PVDF-HFP membrane. However, after fluorination, the reduced surface energy of the PVDF-HFP-F membrane, together with the re-entrant structure of nanofibrous structure could endow a metastable Cassie-Baxter state with the composite liquid-solid-air interface (Fig. 1B), in which the entrapped air can help to support the liquids thus to prevent the membrane pores from being wetted by the feed solution. To quantify the wetting state of membranes within the Cassie-Baxter state, the solid-liquid contact area fraction (f_s) on the PVDF-HFP and PVDF-HFP-F electrospun nanofiber membranes were evaluated (Table S1). The result indicated that when using DI water as the feed solution, the f_s value decreased from (11.3 ± 0.1)% of the PVDF-HFP membrane to (8.9 ± 0.1)% of the PVDF-HFP-F membrane, while decreased from (45.9 ± 0.3) % to (11.9 ± 0.1)% when using NaCl/SDS mixture solution as the feed solution, which confirm that the anti-wetting property of the membrane is closely related with the value of f_s.

4. Conclusions

In this study, the omniphobic PVDF-HFP-F nanofiber membrane with excellent anti-wetting property for MD was successfully fabricated by employing electrospinning and VD fluorination process. Taking

advantage of the intrinsic re-entrant surface texture of the PVDF-HFP nanofiber membrane, an effective VD fluorination process based on physical interaction was investigated. The fabricated fluorinated membrane showed anti-wetting properties against low-surface-tension liquids. The resultant omniphobicity of the PVDF-HFP-F membrane was stable even at harsh conditions such as ultrasonic, boiling water, acid and base treatment. More importantly, the omniphobic PVDF-HFP-F membrane exhibited robust anti-wetting performance in a dynamic DCMD process desalinating surfactant-containing saline feed. The facile method present in this study provides an effective approach for fabricating omniphobic membranes, which could extend the application of MD for treating saline wastewater containing low surface tension contaminants such as surfactants and organic solvents.

Author statement

Xiao-Qiong Wu: Conceptualization, Methodology, Investigation, Writing - Original Draft.

Xing Wu: Investigation, Writing - Original Draft.

Ting-Yu Wang: Validation, Writing - Review & Editing.

Lihua Zhao: Writing - Review & Editing.

Yen Bach Truong: Resources.

Derrick Ng: Resources.

Yu-Ming Zheng: Conceptualization, Writing - Review & Editing, Supervision.

Zongli Xie: Conceptualization, Methodology, Project administration, Writing - Review & Editing, Supervision.

Declaration of competing interest

The authors declare that they have no known competing financial interests or personal relationships that could have appeared to influence the work reported in this paper.

Acknowledgments

Appendix A. Supplementary data

Supplementary data to this article can be found online at https://doi.org/10.1016/j.memsci.2020.118075.

References

[1] N.G.P. Chew, S. Zhao, C. Malde, R. Wang, Polyvinylidene fluoride membrane modification via oxidant-induced dopamine polymerization for sustainable direct-contact membrane distillation, J. Membr. Sci. 563 (2018) 31–42.

[2] S. Alobaidani, E. Curcio, F. Macedonio, G. Diprofio, H. Alhinai, E. Drioli, Potential of membrane distillation in seawater desalination: thermal efficiency, sensitivity study and cost estimation, J. Membr. Sci. 323 (2008) 85–98.

[3] P. Wang, T.-S. Chung, Recent advances in membrane distillation processes: membrane development, configuration design and application exploring, J. Membr. Sci. 474 (2015) 39–56.

[4] E. Drioli, A. Ali, F. Macedonio, Membrane distillation: recent developments and perspectives, Desalination 356 (2015) 56–84.

[5] A. Alkhudhiri, N. Darwish, N. Hilal, Membrane distillation: a comprehensive review, Desalination 287 (2012) 2–18.

[6] A. Deshmukh, C. Boo, V. Karanikola, S. Lin, A.P. Straub, T. Tong, D.M. Warsinger, M. Elimelech, Membrane distillation at the water-energy nexus: limits, opportunities, and challenges, Energy Environ. Sci. 11 (2018) 1177–1196.

[7] C.R. Martinetti, A.E. Childress, T.Y. Cath, High recovery of concentrated RO brines using forward osmosis and membrane distillation, J. Membr. Sci. 331 (2009) 31–39.

[8] S. Lin, S. Nejati, C. Boo, Y. Hu, C.O. Osuji, M. Elimelech, Omniphobic membrane for robust membrane distillation, Environ. Sci. Technol. Lett. 1 (2014) 443–447.

[9] M. Rezaei, D.M. Warsinger, V.J. Lienhard, M.C. Duke, T. Matsuura, W.M. Samhaber, Wetting phenomena in membrane distillation: mechanisms, reversal, and prevention, Water Res. 139 (2018) 329–352.

[10] E.J. Lee, B.J. Deka, J. Guo, Y.C. Woo, H.K. Shon, A.K. An, Engineering the Re-entrant Hierarchy and surface energy of PDMS-PVDF membrane for membrane distillation using a facile and benign microsphere coating, Environ. Sci. Technol. 51 (2017) 10117–10126.

[11] Z. Wang, S. Lin, Membrane fouling and wetting in membrane distillation and their mitigation by novel membranes with special wettability, Water Res. 112 (2017) 38–47.

[12] Y.X. Huang, Z. Wang, J. Jin, S. Lin, Novel janus membrane for membrane distillation with simultaneous fouling and wetting resistance, Environ. Sci. Technol. 51 (2017) 13304–13310.

[13] Y.-X. Huang, Z. Wang, D. Hou, S. Lin, Coaxially electrospun super-amphiphobic silica-based membrane for anti-surfactant-wetting membrane distillation, J. Membr. Sci. 531 (2017) 122–128.

[14] Y. Liao, R. Wang, A.G. Fane, Engineering superhydrophobic surface on poly (vinylidene fluoride) nanofiber membranes for direct contact membrane distillation, J. Membr. Sci. 440 (2013) 77–87.

[15] C. Boo, J. Lee, M. Elimelech, Engineering surface energy and nanostructure of microporous films for expanded membrane distillation applications, Environ. Sci. Technol. 50 (2016) 8112–8119.

[16] J. Lee, C. Boo, W.H. Ryu, A.D. Taylor, M. Elimelech, Development of omniphobic desalination membranes using a charged electrospun nanofiber scaffold, ACS Appl. Mater. Interfaces 8 (2016) 11154–11161.

[17] S. Martin, P.S. Brown, B. Bhushan, Fabrication techniques for bioinspired, mechanically-durable, superliquiphobic surfaces for water, oil, and surfactant repellency, Adv. Colloid Interface Sci. 241 (2017) 1–23.

[18] A. Tuteja, W. Choi, J.M. Mabry, G.H. McKinley, R.E. Cohen, Robust omniphobic surfaces, Proc. Natl. Acad. Sci. U.S.A. 105 (2008) 18200–18205.

[19] R. Zheng, Y. Chen, J. Wang, J. Song, X.-M. Li, T. He, Preparation of omniphobic PVDF membrane with hierarchical structure for treating saline oily wastewater using direct contact membrane distillation, J. Membr. Sci. 555 (2018) 197–205.

[20] L.-H. Chen, A. Huang, Y.-R. Chen, C.-H. Chen, C.-C. Hsu, F.-Y. Tsai, K.-L. Tung, Omniphobic membranes for direct contact membrane distillation: effective deposition of zinc oxide nanoparticles, Desalination 428 (2018) 255–263.

[21] H. Shan, J. Liu, X. Li, Y. Li, F.H. Tezel, B. Li, S. Wang, Nanocoated amphiphobic membrane for flux enhancement and comprehensive anti-fouling performance in direct contact membrane distillation, J. Membr. Sci. 567 (2018) 166–180.

[22] M. Wang, G. Liu, H. Yu, S.H. Lee, L. Wang, J. Zheng, T. Wang, Y. Yun, J.K. Lee, ZnO nanorod array modified PVDF membrane with superhydrophobic surface for vacuum membrane distillation application, ACS Appl. Mater. Interfaces 10 (2018) 13452–13461.

[23] B.S. Lalia, E. Guillen-Burrieza, H.A. Arafat, R. Hashaikeh, Fabrication and characterization of polyvinylidenefluoride-co-hexafluoropropylene (PVDF-HFP) electrospun membranes for direct contact membrane distillation, J. Membr. Sci. 428 (2013) 104–115.

[24] Y. Liao, R. Wang, M. Tian, C. Qiu, A.G. Fane, Fabrication of polyvinylidene fluoride (PVDF) nanofiber membranes by electro-spinning for direct contact membrane distillation, J. Membr. Sci. 425–426 (2013) 30–39.

[25] C. Feng, K.C. Khulbe, T. Matsuura, R. Gopal, S. Kaur, S. Ramakrishna, M. Khayet, Production of drinking water from saline water by air-gap membrane distillation using polyvinylidene fluoride nanofiber membrane, J. Membr. Sci. 311 (2008) 1–6.

[26] J.A. Prince, G. Singh, D. Rana, T. Matsuura, V. Anbharasi, T. S. Shanmugasundaram, Preparation and characterization of highly hydrophobic poly(vinylidene fluoride) – clay nanocomposite nanofiber membranes (PVDF–clay NNMs) for desalination using direct contact membrane distillation, J. Membr. Sci. 397–398 (2012) 80–86.

[27] L.D. Tijing, J.-S. Choi, S. Lee, S.-H. Kim, H.K. Shon, Recent progress of membrane distillation using electrospun nanofibrous membrane, J. Membr. Sci. 453 (2014) 435–462.

[28] L. Zhao, C. Wu, X. Lu, D. Ng, Y.B. Truong, Z. Xie, Activated carbon enhanced hydrophobic/hydrophilic dual-layer nanofiber composite membranes for high-performance direct contact membrane distillation, Desalination 446 (2018) 59–69.

[29] X. Li, H. Shan, M. Cao, B. Li, Facile fabrication of omniphobic PVDF composite membrane via a waterborne coating for anti-wetting and anti-fouling membrane distillation, J. Membr. Sci. 589 (2019) 117262.

[30] L. Deng, L. Ye, X. Li, P. Li, J. Zhang, X. Wang, M. Zhu, B.S. Hsiao, Self-roughened omniphobic coatings on nanofibrous membrane for membrane distillation, Separ. Purif. Technol. 206 (2018) 14–25.

[31] X. An, Z. Liu, Y. Hu, Amphiphobic surface modification of electrospun nanofibrous membranes for anti-wetting performance in membrane distillation, Desalination 432 (2018) 23–31.

[32] C. Boo, J. Lee, M. Elimelech, Omniphobic polyvinylidene fluoride (PVDF) membrane for desalination of shale gas produced water by membrane distillation, Environ. Sci. Technol. 50 (2016) 12275–12282.

[33] Y.B. Truong, Y. O'Bryan, I.D. McKelvie, I.L. Kyratzis, W. Humphries, Application of electrospun gas diffusion nanofibre-membranes in the determination of dissolved carbon dioxide, Macromol. Mater. Eng. 298 (2013) 590–596.

[34] R.N. Shimizu, N.R. Demarquette, Evaluation of surface energy of solid polymers using different models, J. Appl. Polym. Sci. 76 (2000) 1831–1845.

[35] D.K. Owens, R. Wendt, Estimation of the surface free energy of polymers, J. Appl. Polym. Sci. 13 (1969) 1741–1747.

[36] K.J. Lu, Y. Chen, T.S. Chung, Design of omniphobic interfaces for membrane distillation - a review, Water Res. 162 (2019) 64–77.

[37] T.L. Liu, C.-J.C. Kim, Turning a surface superrepellent even to completely wetting liquids, Science 346 (2014) 1096–1100.

[38] L. Wang, Y. Zhao, Y. Tian, L. Jiang, A general strategy for the separation of immiscible organic liquids by manipulating the surface tensions of nanofibrous membranes, Angew. Chem., Int. Ed. Engl. 54 (2015) 14732–14737.

[39] X. Li, X. Yu, C. Cheng, L. Deng, M. Wang, X. Wang, Electrospun superhydrophobic organic/inorganic composite nanofibrous membranes for membrane distillation, ACS Appl. Mater. Interfaces 7 (2015) 21919–21930.

[40] H. Ma, C. Burger, B.S. Hsiao, B. Chu, Ultra-fine cellulose nanofibers: new nano-scale materials for water purification, J. Mater. Chem. 21 (2011) 7507.

[41] H. Zhou, H. Wang, H. Niu, Y. Zhao, Z. Xu, T. Lin, A waterborne coating system for preparing robust, self-healing, superamphiphobic surfaces, Adv. Funct. Mater. 27 (2017) 1604261.

[42] H. Zhou, H. Wang, H. Niu, T. Lin, Electrospun fibrous membranes with super-large-strain electric superhydrophobicity, Sci. Rep. 5 (2015) 15863.